# Adsorption Mechanism of Microcrystalline Cellulose as Green Adsorbent for the Removal of Cationic Methylene Blue Dye

[1]Kok Bing Tan, [2]Ahmad Zuhairi Abdullah, [1,3]Bahman Amini Horri and [1]Babak Salamatinia*
[1]*Chemical Engineering Discipline, School of Engineering, Monash University Malaysia, Jalan Lagoon Selatan, Bandar Sunway, 47500 Selangor, Malaysia.*
[2]*School of Chemical Engineering, Engineering Campus, Universiti Sains Malaysia, 14300, Nibong Tebal, Penang, Malaysia.*
[3]*Department of Chemical & Process Engineering, Faculty of Engineering and Physical Sciences, University of Surrey, Surrey GU2 7XH, United Kingdom.*
babak.salamatinia@monash.edu*

(Received on 24th August 2015, accepted in revised form 10th March 2016)

**Summary**: The adsorption mechanism of pure cellulose is yet to be explored. Thus, in this study, the adsorption mechanism of Microcrystalline Cellulose (MCC), a polysaccharide which is renewable, low cost and non-toxic, was studied on the adsorption of model dye Methylene blue (MB). It was found that the main adsorption mechanism of MB on MCC was due to the electrostatic attraction between the positively charged MB dye and negatively charged MCC. Thus, physical adsorption was the dominant effect, since electrostatic attraction is categorized as physical adsorption. This was verified by Dubinin-Radushkevich isotherm, whereby mean free energy adsorption value was found to be less than 8 kJ/mol. The values of Gibbs free energy for thermodynamics studies were found to be within the range of -20 kJ/mol and 0 kJ/mol, which also indicated physical adsorption. It was due to the electrostatic attraction as adsorption mechanism of this adsorption process which resulted rapid adsorption of MB dye. It was found that equilibrium dye concentration was achieved between 1-3 minutes, depending on the adsorption temperature. The rapid adsorption, as compared to a lot of materials, showed the potential of MCC as the future of green adsorbent. The adsorption of Methylene Blue on MCC fitted well in Langmuir Isotherm, with $R^2$ values of higher than 0.99, while fitted moderately in Freundlich Isotherm, with $R^2$ values between 0.9224 and 0.9223. Comparatively, the adsorption of MB on MCC fitted best Langmuir Isotherm as compared to Freundlich Isotherm which monolayer adsorption occurred at the homogenous surface of MCC. This also indicated adsorbed MB molecules do not interact with each other at neighboring adsorption sites. The maximum adsorption capacity calculated from Langmuir Isotherm was found to be 4.95 mg/g. Despite the potential of MCC as green adsorbent, the challenge of low adsorption capacity has to be addressed in the future.

Keyword: Green Adsorbent, Microcrystalline Cellulose, Adsorption Mechanism, Sustainable, Low cost, Methylene Blue.

## Introduction

Small amount of dye in water is highly visible and significantly affect aquatic life due to carcinogenic and mutagenic properties of dyes [1]. Therefore, it is of utmost importance to remove dye efficiently to ensure safe discharge into the environment. Techniques such as coagulation [2], membrane filtration [3], electro-catalytic method [4] and adsorption [5-10] are commonly utilized for the removal of dyes. Adsorption is found to be effective, cheap, simple, and relatively lower operation cost of dye removal [11]. Different types of materials have been developed as adsorbents for effective adsorption of dye. In recent years, developments of polysaccharides-based green adsorbents received widespread attention as they are valued for their renewability, low cost and non-toxicity [12]. Direct use of polysaccharides such as maize straw [13], palm oil biomass [14], chitosan [15] and many other polysaccharides- based adsorbents; have been studied as potential effective yet renewable adsorbent. At the same time, isotherm, kinetics and thermodynamics studies were also conducted on these adsorbents to study the adsorption mechanism of these adsorbents.

Throughout the years, several modifications on these polysaccharides have been studied to improve the mechanical, chemical and physical properties of the adsorbent in order to increase the adsorption capacities of dyes. Modification techniques such as cross-linking and grafting are widely used to modify polysaccharides-based adsorbents such as chitosan [16-18] and cellulose [19-22]. These modifications might play a significant role in determining the adsorption mechanism, isotherm, kinetics and thermodynamics, which might be different as compared to pure chitosan and pure cellulose. However, to our knowledge, there is very limited information about the adsorption mechanism,

*To whom all correspondence should be addressed.

isotherm, kinetics and thermodynamics on the adsorption of dyes using pure cellulose as adsorbent.

Therefore, this paper focused on the study of adsorption mechanism, isotherm, kinetics and thermodynamics on the adsorption of dyes using pure cellulose as potential renewable green adsorbent. The effects of initial concentrations, contact time, pH and temperatures on the dye adsorption performance using pure cellulose were also evaluated. Characterization tests on pure cellulose samples before and after adsorption were also conducted to explain the adsorption performance and mechanism of pure cellulose. Micro-crystalline Cellulose (MCC) was chosen as pure cellulose for this study as it is a readily available commercial source, and could be used directly on the adsorption of dyes without any modification or pre-treatment. For the case study to investigate the potential of pure cellulose as adsorbent, Methylene blue (MB), was chosen as a model dye for adsorption, as it is usually used as a model component for organic components and dyes removal from aqueous solution [23].

## Experimental

### *Materials*

Methylene Blue MB, with dye contents of 82 %, was obtained from Sigma Aldrich Ltd. (USA). Meanwhile, MCC, with and average particle diameter of 50 µm was supplied by FMC BioPolymer, USA (Avicel PH-102). $HNO_3$ and NaOH; both supplied by Sigma Aldrich Ltd. (USA), were diluted to 0.1M to be used to study the effect of pH on the dye percentage removal. All the chemicals used were of Analytical grade and were stored in a dry cabinet to avoid any changes due to humidity.

### *Dye Adsorption Studies*

Different concentrations of MB dye solution were prepared by diluting desired amount of dye in distilled water. Dye adsorption experiments were conducted as batch tests in 100 ml conical flasks. Without further modification, a desired amount of MCC was added to 50 ml of dye solution and was mixed. Sampling was done using an Eppendorf micro-pipette at fixed time intervals of 30 seconds. The sample was then centrifuged at 6000 rpm for 1 minute in a mini centrifuge (Scan Speed Mini Centrifuge, USA) to remove the MCC from the dye solution. The aqueous solution was then tested for concentration of MB without any further delay using a UV-Vis spectrophotometer (Thermo Genesys 10UV, USA). The absorbance value measured was directly proportional to dye concentration according to Beer-Lambert Law [24]. A calibration curve for MB plotted beforehand at 663 nm of wavelength to be used as reference. Initial and changes of dye concentrations were reported in percentage removal and adsorption capacity ($Q_e$). The percentage removal was obtained based on Eq. (1) as follow:

$$Percentage\ Removal,(\%) = \left(C_0 - C_f\right)/C_0 \times 100 \quad (1)$$

whereby, $C_o$ is the initial dye concentration, $C_f$ shows the final dye concentration. Meanwhile, the adsorption capacity is obtained based on Eq. (2) as followed:

$$Q_e = (C_0 - C_f)V/m \quad (2)$$

whereby, $C_o$ stands for the dye concentration, $C_f$ is the final dye concentration, $Q_e$ identifies the adsorption capacity, V is volume of dye solution and, m represents the mass of MCC adsorbent. All the experiments were repeated three times for each set of parameters to ensure accuracy and reproducibility of results, and the average values are reported.

The effects of the four parameters were investigated. These include dye initial concentration (1 ppm-15 ppm), adsorbent dosage (1 g/L-9 g/L), pH (2-11), temperature (298 K-308 K) and time (0-18 min).

### *Characterization*

### *Zetasizer and Potential*

The surface charges or zeta potentials of MCC in a pH range of 2-10 were measured using Malvern Zetasizer Series, UK. MCC was mixed in distilled water, and the pH was adjusted using 0.1 M of $HNO_3$ and 0.1 M of NaOH.

### *Brunauer–Emmet–Teller (BET)*

The specific surface area and porosity of MCC was measured using the Brunauer–Emmet–Teller (BET) method. By using ASAP 2020 Surface Analyzer by Micrometrics, USA the specific area and porosity were obtained with adsorption of $N_2$ at $77 \pm 0.5$ K. Prior to analysis, the sample was degassed under vacuum at 90 °C for 12 hours. The holding temperature was 200°C for 4 hours reaction time.

*Field Emission Scanning Electron Microscope (FE-SEM)*

The morphological features of the surface for MCC, MB powder, and MCC containing adsorbed MB were observed using Field Emission Scanning Electron Microscope (FE-SEM) Hitachi SU8000, Japan at an accelerating voltage of 2 kV. Samples were coated with platinum before observation as MCC is conductive.

*Fourier Transform Infrared (FTIR) Spectroscopy*

The chemical structure and functional groups of the samples were analyzed using Fourier Transform Infrared (FTIR) Spectroscopy (Thermo Scientific Nicolet IS10). The powders were placed in a pastille of KBr. The samples which were used include MCC powder, MB powder and MCC powder containing adsorbed MB.

**Results and Discussion**

*Effect of Initial Concentration*

Fig. 1 shows the percentage removal and adsorption capacity of MB with initial dye concentrations of 1ppm to 15 ppm. The adsorbent dosage was fixed at 5 g/L at a temperature of 298 K and pH of 6. As shown in Fig. 1, the percentage removal decreased from 93% to 81%, as the initial concentration increased. For a fixed adsorbent dosage, the amount of adsorption sites for incoming MB molecules are fixed, and could only accommodate a limited amount of MB molecules. By increasing the dye initial concentration; there will be more excess MB molecules that could not be adsorbed due to limited amount of adsorption sites, resulting in decreasing percentage removal of MB [25].

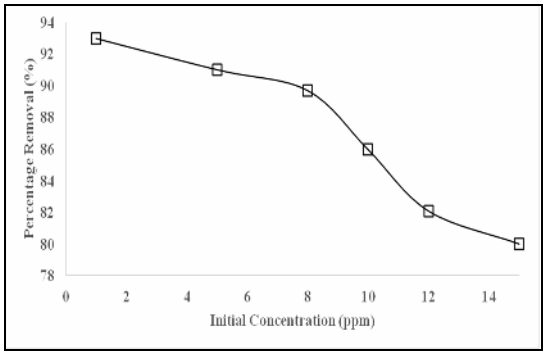


Fig. 1: Effect of Initial Concentration of MB on MB dye removal (MCC dosage 5g/L, Temperature 298K, pH 6).

*Effect of Adsorbent Dosage*

The investigation on the effect of adsorbent dosage was mainly concern with the ability of dye being adsorbed with the smallest amount of adsorbent, subsequently to investigate the capability of dye adsorption with economical view [26]. Fig. 2 shows the effect of different MCC adsorbent dosage on dye percentage removal at equilibrium. For a fixed amount of dye, the dye percentage removal increased with increasing adsorbent dosage, as there were more adsorption sites available for MB dye molecules [26]. Therefore the adsorption sites were able to achieve saturation at higher dye percentage removal [27]. As a result, the dye percentage removal increased significantly from 40% to 80% as the adsorbent dosage increases from 1 g/L to 3g/L, as shown in Fig. 2. Meanwhile, beyond 3 g/L, there was insignificant increased in dye percentage removal. Therefore, in an economical point of view, the optimum adsorbent dosage is determined to be 3 g/L for efficient dye removal.

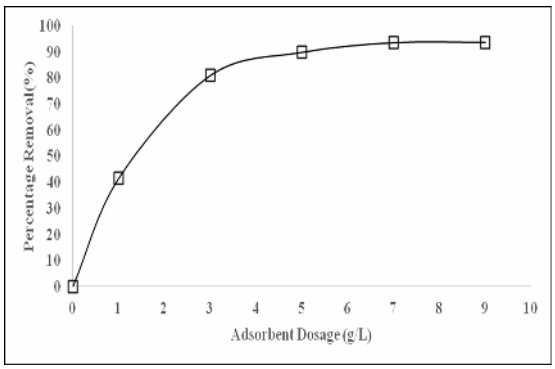


Fig. 2: Effect of Adsorbent Dosage on MB dye removal (Initial Concentration 8ppm, Temperature 298K, pH 6).

*Effect of pH*

Fig. 3 shows the effect of dye pH between the ranges of 2-10 on the percentage removal of MB dye. Highest efficiency of dye removal was observed in Fig. 3 at the range of pH 4-10, achieving dye percentage removal of at least 85%. Efficient removal of dye at these wide ranges of pH values indicated that MCC could be potentially used to treat industrial textile dyes wastewater, which typically has pH values between 7 to 8 [28].

Dye percentage removal decreased significantly as the pH decreases below pH 4. At low pH of 2, the percentage removal of dye was the lowest, which is 42%. Similar trends of results were also reported on the removal of MB using other cellulosic-based materials such as garlic peel [29], *Posidonia Oceania* fiber [30], passion fruit peel [31] and pineapple leaf powder [32]. These trends of results can be explained by studying the zeta potential values of MCC at different pH, which is shown in Fig. 4 the isoelectric point of MCC was at pH 2.8. This indicated that MCC was generally negatively charge at wide range of pH. Similar zeta potential trend was also reported and predicted by Zhukov et.al [33] by using Smoluchowski and Henry Equations. Based on Fig. 4 MCC had net positive zeta potential values at pH 2 due to high concentration of $H^+$ ion. As a result, incoming cationic MB molecules were repelled from the adsorption surface of MCC due to electrostatic repulsion [6]. Therefore, lowest dye percentage removal was obtained at this pH value. Beyond isoelectric point of pH 2.8, the negatively charged MCC resulted in significant increase in dye removal as the pH increased from pH 2 to pH 4, as shown in Fig. 3. Thus, it was proposed that the adsorption mechanism of MB on MCC involved electrostatic attraction. The same adsorption mechanism was also used to explain the trend of results in other cellulosic materials like garlic peel, *Posidonia Oceania* fiber, passion fruit peel and pineapple leaf powder [29-32] for the adsorption of MB.

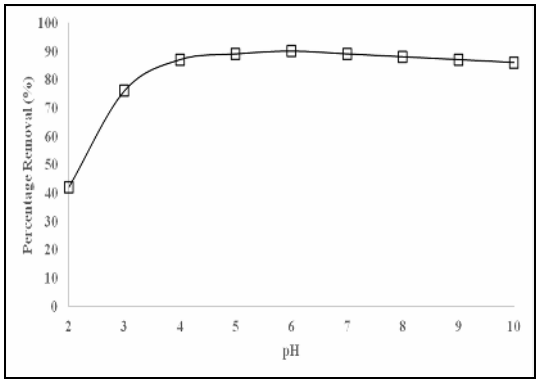


Fig. 3: Effect of pH on the percentage removal of MB (Initial Concentration 5ppm, adsorbent dosage 5g/L, Temperature 298K).

*Equilibrium Studies and Adsorption Isotherm*

Section 3.1-Section 3.3 has discussed the effects of different adsorption conditions on the removal of MB. However, in order for successful application of adsorption for practical usage, adsorption isotherms studies on various models were essential to study the in-depth behavior of MCC as an adsorbent. Fig. 5 shows the equilibrium curves of adsorption capacity at equilibrium ($Q_e$) vs Equilibrium Concentration ($C_e$). In order to obtain a more accurate description on equilibrium curve, the dye initial concentrations were expanded to 25 ppm, 50 ppm, 75 ppm and 100 ppm. Based on Fig. 5, all the equilibrium curves at different temperatures are of "H2" type isotherm, according to Giles et al. [34] classification. These results indicated that MB dye molecules have very high affinity for MCC surface, resulted in complete adsorption in dilute dye solution [35]. Limosin et al. [36] stated that "H" type of isotherm generally obey Langmuir, Freundlich or Temkin Isotherms. Therefore, the equilibrium data were fitted at these three isotherm modelling.

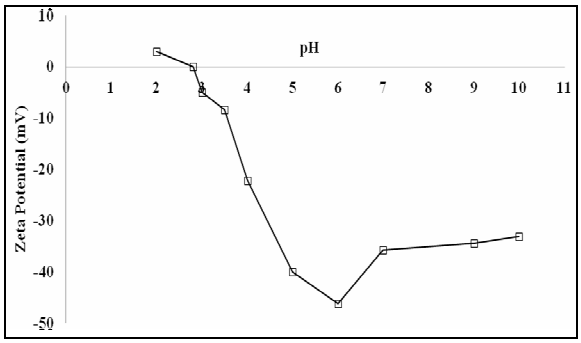


Fig. 4: Zeta Potential of MCC.

Langmuir Isotherm, first described by Langmuir [37], is modeled based on the assumption that monolayer adsorption occur on homogenous sites and surface of the adsorbent, whereby no further adsorption could take place on adsorption sites once they are occupied. Besides that, there is no interaction between molecules adsorbed on neighboring sides. The linearized Langmuir Isotherm is derived based on the Eq. (3):

$$\frac{C_e}{Q_e} = \frac{\frac{C_e}{Q_{max}+1}}{K_L Q_{max}} \quad (3)$$

whereby $Q_e$ is the adsorption capacity at equilibrium, $C_e$ is the equilibrium concentration of adsorbate (mg/L), $K_L$ is the Langmuir isotherm constant (L/mg), and $Q_{max}$ is the maximum adsorption

capacity for Langmuir isotherm. Another important feature of Langmuir model Isotherm is the separation parameter, $R_L$, which is defined in Eq. (4) [38]:

$$R_L = \frac{1}{1 + K_L C_{max}} \quad (4)$$

whereby, $C_{max}$ is the highest dye concentration used in this experiment. The value of $R_L$ indicates to be either unfavorable ($R_L$>1), linear ($R_L$=1), favorable (0<$R_L$<1) and irreversible ($R_L$=0).

Freundlich isotherm [39] is modeled based on the assumption that multilayer adsorption occurs on heterogeneous sites and surface of the adsorbent, whereby reversible adsorption occurred. Besides that, there is interaction between molecules adsorbed on neighboring sides. The linearized Freundlich Isotherm is derived as Eq. (5):

$$Ln Q_e = Ln K_f + \left(\frac{1}{n}\right) Ln C_e \quad (5)$$

Temkin Isotherm is modelled based on the assumption that the decreased of heat of adsorption as a function of temperature is linear instead of logarithmic [40]. Linearized Temkin Isotherm is derived based on Eq. (6):

$$Q_e = B_T Ln K_T + B_T Ln C_e \quad (6)$$

where, $K_T$ represents the Temkin isotherm equilibrium binding constant and $B_T$ is Temkin isotherm constant associated with adsorbate-adsorbate interaction and adsorption heat $\Delta H_T$, whereby $B_T$= -RT/ $\Delta H_T$ [41], with R is the universal gas constant of 8.314 J/K/mol, and T is the temperature in kelvin scale [42]. Therefore, Temkin isotherm is a function to temperature. Adsorption heat $\Delta H_T$ is essential to determine whether MCC adsorbent behave as a physical adsorption or chemisorption [41].

On top of these three isotherm model, Dubinin-Radushkevich Isotherm is also essential to determine whether MCC adsorbent behave as a physical adsorption or chemisorption. This is because Dubinin-Radushkevich isotherm can be used for the estimation of apparent free energy and the characteristics of adsorption [40]. Thus, Dubinin-Radushkevich Isotherm is also used to fit the equilibrium data. Linearized Dubinin-Radushkevich Isotherm is derived based on Eq. (7):

$$Ln Q_e = Ln Q_m - B\varepsilon^2 \quad (7)$$

where, B denotes the Dubinin-Radushkevich isotherm constant associated with adsorption energy, $Q_m$ is the Dubinin-Radushkevich adsorption capacity and Ɛ represents the Polanyi potential, derived from Eq. (8):

$$\varepsilon = RT Ln\left(1 + \frac{1}{C_e}\right) \quad (8)$$

The mean free energy adsorption $E_a$ could be determine based on the Dubinin-Radushkevich isotherm constant B, derived in Eq. (9).

$$E_a = \frac{1}{\sqrt{2B}} \quad (9)$$

Based on Eq. (4), (5), (6) and (7), the corresponding characteristics parameters are tabulated in $Q_{max}$ and $K_L$ could be obtained from the slope and the intercept respectively from the linearized Langmuir isotherm in Fig. 6, the equilibrium data fitted well in Langmuir Isotherm at all temperatures, with $R^2$ ranging from 0.994-0.9977. Compared to Freundlich, Temkin and Dubinin-Radushkevich isotherms, Langmuir isotherms had the highest $R^2$ values at all temperature. Thus, the adsorption of MB on MCC was based on monolayer adsorption at the homogenous surface of MCC, whereby adsorbed MB molecules did not interact with each other at neighboring adsorption sites. As shown in Fig. 5, the maximum adsorption capacity $Q_{max}$ decreased with temperature, which is further discussed in Section 3.5. Table-1 also tabulates the separation parameter $R_L$, which are shown to be within 0<$R_L$<1, which confirmed a favorable adsorption process at all temperatures.

$K_f$ and 1/n could be obtained from the intercept and slope of the Linearized Freundlich Isotherm respectively in Fig. 7. $K_f$, which is related to Freundlich adsorption capacities, was shown to decrease with temperature, and has a similar trend with $Q_{max}$ from Langmuir Isotherm. As observed in Table-1, all the 1/n values ranged between 0.1 and 1 at all temperatures. This suggests that the adsorption of MB on MCC is favorable at all temperatures [43], supported by the $R_L$ values based on Langmuir Isotherm.

The equilibrium data did not fitted well in Temkin and Dubinin-Radushkevich isotherms modelling, as evident by their lower $R^2$ values

compared to Langmuir Isotherms. However, despite their low $R^2$ values, Temkin and Dubinin-Radushkevich isotherms could give insights on the adsorption mechanisms [44], based on adsorption heat $\Delta H_T$ and mean free energy adsorption $E_a$, respectively. As could be observed in Table-2, the adsorption heat ΔHT were -3.25 kJ/mol, -3.61 kJ/mol and -5.42 kJ/mol at 298 K, 308 K and 318 K respectively. The adsorption heat values at all the temperatures were higher than -20 kJ/mol; suggesting that physical adsorption is the dominant effect [45] behind the adsorption mechanism of MB on MCC. Similarly, the mean free energy adsorption $E_a$ values at different temperatures as shown in Table-2, are less than 8 kJ/mol, suggesting that physical adsorption [43] is the dominant effect behind the adsorption mechanism of MB on MCC. These verified the deduction on Section 3.3 that the adsorption of MB on MCC was mainly physical adsorption, which was attributed to rely on electrostatic attraction between MCC and MB.

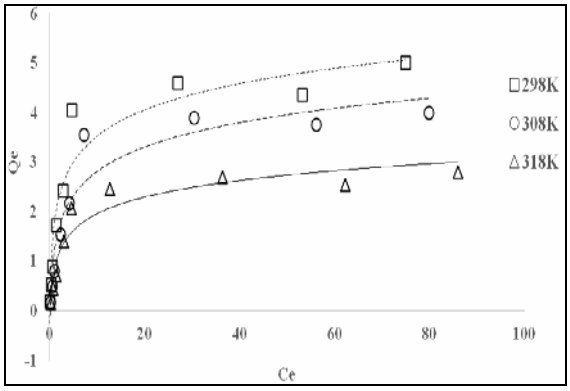


Fig. 5: Equilibrium Curves at different temperatures.

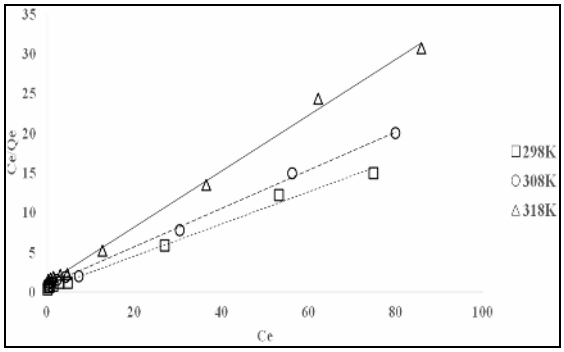


Fig. 6*:* Linearized Langmuir Isotherm.

Table-1: Isotherm Parameters values at different temperature.

| Model | Parameters | Temperature | | |
|---|---|---|---|---|
| | | 298K | 308K | 318K |
| Langmuir | $Q_{max}$(mg/g) | 4.95 | 4.14 | 2.84 |
| | $K_L$ (L/mg) | 0.396 | 0.282 | 0.299 |
| | $R_L$ | 0.02 | 0.03 | 0.03 |
| | $R^2$ | 0.994 | 0.9977 | 0.9966 |
| Freundlich | $K_f$ (mg/g) | 5.88 | 3.25 | 2.29 |
| | 1/n | 0.7576 | 0.7092 | 0.4878 |
| | $R^2$ | 0.9231 | 0.9227 | 0.9224 |
| Temkin | $B_T$ (L/mg) | 0.7612 | 0.7096 | 0.4876 |
| | $K_T$ | 10.32 | 5.26 | 5.49 |
| | $\Delta H_T$(kJ/mol) | -3.25 | -3.61 | -5.42 |
| | $R^2$ | 0.9231 | 0.9227 | 0.9224 |
| Dubinin-Radushkevich | $Q_m$(mg/g) | 2.86 | 2.49 | 1.92 |
| | B($mol^2/kJ^2$) | 0.0674 | 0.1245 | 0.1485 |
| | $E_a$ (kJ/mol) | 2.72 | 2 | 1.83 |
| | $R^2$ | 0.7633 | 0.7848 | 0.8102 |

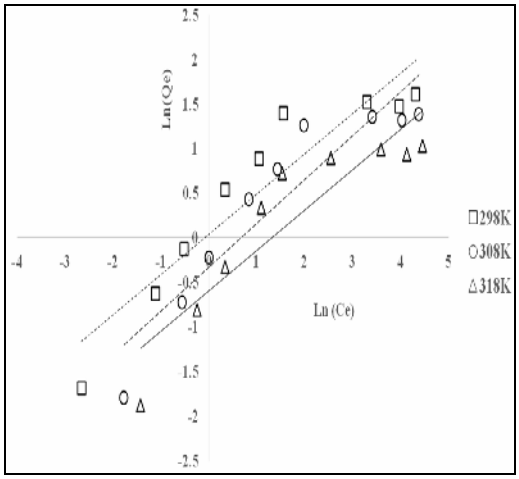


Fig. 7: Linearized Freundlich Isotherm.

*Effect of Temperature on Equilibrium and Thermodynamics Studies*

Thermodynamics studies were essential to study the spontaneous of the process with temperature, by taking into considerations into both energy and entropy. This was performed by using the Van Hoff's equation, which is derived below as Eq. (10):

$$LnK_c = Ln\left(\frac{Q_e}{C_e}\right) = -\frac{\Delta G}{RT} = -\frac{\Delta H}{RT} + \frac{\Delta S}{R} \quad (10)$$

whereby, $K_c$ is the equilibrium constant, ΔH is the change in enthalpy, ΔS is the change in entropy and ΔG is the Gibbs free energy. A plot of Ln $K_c$ vs 1/T was plotted (not shown) and the value of ΔH and ΔS was obtained from the intercept and slope of the plot respectively. These values were tabulated in Table-2.

Looking into results presented in Table-2, ΔG values at all temperatures were in negative values, which confirmed the spontaneous and feasibility of the adsorption of MB dye on MCC [46], thus verified the $R_L$ and 1/n values from Langmuir and Freundlich Isotherms respectively. Furthermore, the ΔG values at all the temperatures were within the range of -20kJ/mol and 0 kJ/mol, further confirmed the deduction in Section 3.3 that physical adsorption [47]was the dominant adsorption mechanism behind the adsorption of MB dye on MCC.

The increasing in ΔG values with temperature and the negative ΔS indicated that the adsorption was spontaneous at lower temperature due to the decrease in randomness occurs with increasing temperature [48]. As a result, the adsorption was exothermic in nature, indicated by the negative ΔH values at all temperatures [20]. The decreased in randomness with temperature resulting in the decrease in adsorption capacities at all dye initial concentration with temperature, as evident in the equilibrium curves in Fig. 5, and the decreased in $Q_{max}$ and Kf values with temperatures from Langmuir and Freundlich Isotherms respectively.

Table-2: Thermodynamics Parameters.

| Temperature | ΔG (KJ/mol) | $K_c$ | ΔH (kJ/mol) | ΔS (J/mol) |
|---|---|---|---|---|
| 298K | -5.44 | 9.00 | | |
| 308K | -3.97 | 4.71 | -32.1 | -90.2 |
| 318K | -3.67 | 4.00 | | |

*Effect of Contact Time and Adsorption Kinetics*

The effects of contact time on the adsorption of MB on the percentage at different temperatures are shown in Fig. 8, the adsorption occurred very rapidly, reaching equilibrium at 3 minutes, 1.5 minutes and 1 minute at 298 K, 308 K, and 318 K respectively. The maximum percentage removals and equilibrium adsorption capacities were achieved at 298 K, 308 K and 318 K are 90%, 85% and 80%, 1.44 mg/g, 1.36 mg/g and 1.28 mg/g respectively.

It should be highlighted that in comparisons to other adsorbents for the adsorption of MB, MCC had a significantly very fast adsorption. This include nanoparticles such as Carbon Nanotubes [49], Ilemite nanoparticles [50] and Titania nanoparticles [51], achieving equilibrium time at 60 minutes, 600 minutes and 90 minutes respectively, and wastes such as pyrolyzed petrified sediments, achieving equilibrium time in 480 minutes [52]. The strong electrostatic attraction enable rapid filling of adsorption sites by MB molecules on the surface of MCC, resulting in a very rapid adsorption rate [53], whereby achieving percentage removal of 66%-74% within 0.5 minutes. However, beyond 0.5 minutes, most of the adsorption sites were occupied, which resulted in decrease in adsorption rate. By 1-3 minutes, all the adsorption sites were occupied [54], whereby saturation and thus maximum percentage removal and equilibrium adsorption capacities had been achieved. Thus, beyond 3 minutes, there was no more further adsorption occurred.

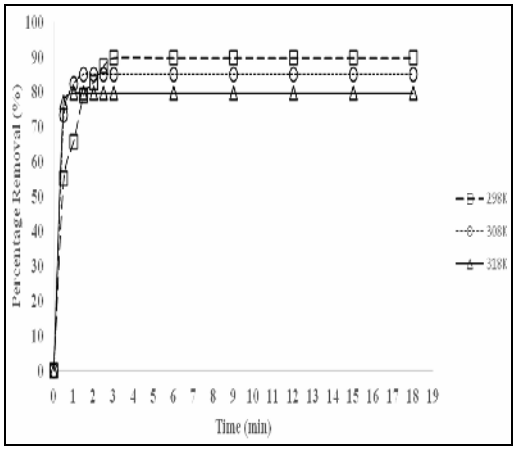


Fig. 8: Effect of contact time of percentage removal of MB at different temperatures (Initial Concentration 8ppm, Adsorbent Dosage 5g/L, pH 6).

Further insight to the adsorption rate could be conducted by evaluating the adsorption kinetics of MB on MCC, which could also determine the rate-determining steps, as well as the adsorption mechanism. Three kinetics models were analyzed, which consist of pseudo-first order, pseudo-second order and Elovorich models. Linearized Pseudo-first order model is defined below in Eq. (11):

$$Ln(Q_e - Q_t) = LnQ_e - K_1 t \quad (11)$$

where, $Q_t$ is the adsorption capacity at time t and $k_1$ is the first order reaction rate constant. Linearized Pseudo-Second Order Model is defined below in Eq. (12):

$$\frac{t}{Q_t} = \frac{1}{k_2 Q_e^2} + \frac{t}{Q_e} \quad (12)$$

whereby, $k_2$ presents the second order reaction rate constant. Linearized Elovorich Kinetics Model is defined below in Eq. (13):

$$Q_t = \beta Ln(\alpha\beta) + \beta Lnt \quad (13)$$

where, α denotes the initial adsorption rate and β represents the constant rate related to surface

coverage and the activation energy for chemical adsorption. Normalized standard deviation (STD) is used to determine the most suitable model that describes the kinetic study of adsorption. Fig. 9 shows the linearized Pseudo-First Order at different temperatures. Clearly, at all the temperatures, the adsorptions of MB dye on MCC did not fit in the Pseudo-first order model at all, as evident with a low $R^2$ values of 0.9851, 0.9743 and 0.9436 at 298 K, 308 K and 318 K respectively, as listed in Table-3. Furthermore, the STD between $Q_{exp}$ (experimental adsorption capacity at equilibrium) and $Q_{cal}$ (calculated adsorption capacity at equilibrium) were very large for all temperatures, which were 10%, 21% and 31% at 298 K, 308 K and 318 K, respectively.

The results obtained from Pseudo-first order model indicated that the adsorption of MB on MCC might follow Pseudo-second order. Fig. 10 shows the linearized Pseudo-second Order at different temperatures. Clearly, at all temperatures, the adsorption of MB on MCC did indeed fit very well in Pseudo-second order model. This was evident with very high $R^2$ values of 0.9997-1 at all temperatures, as listed in Table-3. The STD between $Q_{exp}$ and $Q_{cal}$ were very low for all temperatures, which were 0.5%, 0.05% and 0.02% at 298 K, 308 K and 318 K respectively. Pseudo-second order model is defined based on the rate of adsorption is proportional to the square of the number of unoccupied sites on the adsorption sites on the adsorbate surface as well. Elovorich model is reported to fit very well with adsorption mechanism relating to chemical adsorption [55]. Fig. 11 shows the Linearized Elovorich model at different temperatures. It was observed that the adsorption kinetics of MB adsorption of MCC fitted only moderately with Elovorich model, with $R^2$ were determined to be 0.9863, 0.9876 and 0.9698 at 298 K, 308 K and 318 K respectively as tabulated in Table-3. Since it is only fitted moderately, it is concluded there is no chemical adsorption mechanism involved.

*Characterization*

Characterization was done using FTIR, SEM and XRD and BET surface area, before and after adsorption to better understand and explain the results obtained.

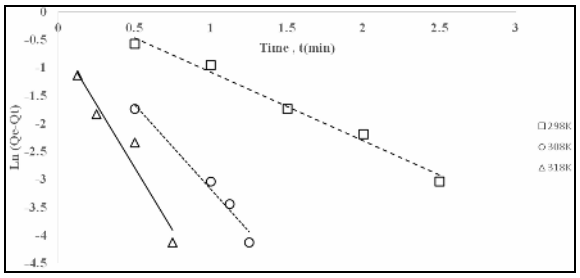


Fig. 9: Linearized Pseudo-First Order.

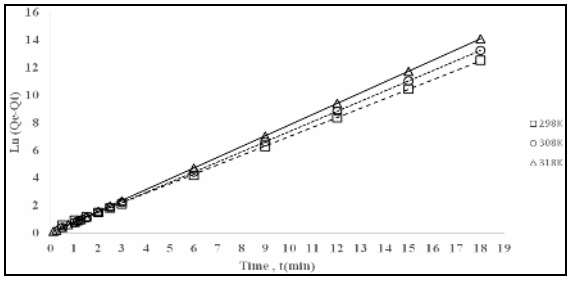


Fig. 10: Linearized Pseudo-Second Order.

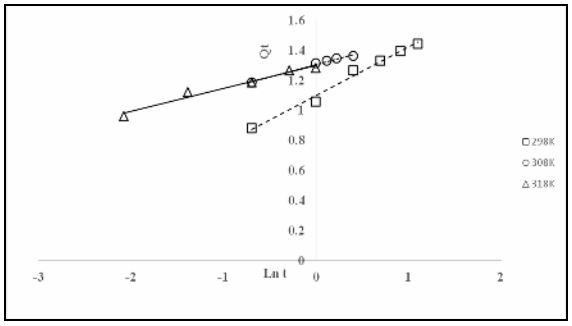


Fig. 11: Linearized Elovorich Model.

Table-3: Kinetics Parameters.

| Model | Parameters | Temperature | | |
|---|---|---|---|---|
| | | 298K | 308K | 318K |
| Pseudo-first Order | $Q_{exp}$ (mg/g) | 1.44 | 1.36 | 1.28 |
| | $Q_{cal}$(mg/g) | 1.15 | 0.85 | 0.58 |
| | $k_1$(min$^{-1}$) | 1.30 | 3.03 | 4.49 |
| | $R^2$ | 0.9851 | 0.9743 | 0.9436 |
| | STD | 10% | 21% | 31% |
| Pseudo-second order | $Q_{exp}$ (mg/g) | 1.440 | 1.360 | 1.280 |
| | $Q_{cal}$ (mg/g) | 1.463 | 1.362 | 1.281 |
| | $k_2$ (g/mg.min) | 3.29 | 34.32 | 59.71 |
| | $R^2$ | 0.9997 | 1 | 1 |
| | STD | 0.5% | 0.05% | 0.02% |
| Elovorich | α (mg/g.min) | 90.74 | 15521.55 | 34714.28 |
| | β (g/mg) | 0.3241 | 0.166 | 0.1513 |
| | $R^2$ | 0.9863 | 0.9876 | 0.9698 |

*BET*

Specific surface area and porosity of MCC were determined using the Brunauer–Emmet–Teller (BET) method. As shown in Table-4, the specific surface area and the pore volume obtained were 1.32 $m^2$/g and 0.02405 $cm^2$/g respectively. The average pore width was 22.72 nm, suggesting that MCC is a mesoporous material [56]. The low specific area of

MCC resulted in a relatively low adsorption capacity of MCC on MB, which is 4.95 mg/g at 298 K. This was despite the fact that MCC could effectively remove MB with high percentage removal due to several adsorption mechanisms. This was because specific surface area correlates to the adsorption capacity and is directly proportional to the number of adsorption sites according to Brunauer–Emmet–Teller (BET) theory [57].

Table-4: BET data for MCC.

| Parameters | Values |
|---|---|
| Specific Surface Area | 1.32 $m^2/g$ |
| Pore Size | 22.72 nm |
| Pore Volume | 0.02405 $cm^3/g$ |

*FE-SEM*

Smooth, crystalline surface was observed on the surface of pure MCC as presented in Fig. 12(a). Meanwhile, Fig. 12(b) shows a sharp-edged, crystallite structure of MB powder, which is significantly different from the MCC surface. Fig. 12(c) is the FE-SEM image for MCC after adsorption of 12 minutes .Compared to Fig. 12 (a), rougher surface was observed for the MCC after adsorption at Fig. 12(c). Several sharp-edged crystalline structures, which indicate the MB particle, are observed to be attached on the surface of MCC due to the dominant electrostatic attraction between the oppositely charged MCC and MB, as verified based on the results of Temkin and Dubinin-Radushkevich Isotherms. The smooth surface of MCC could no longer be observed in Fig. 12(c), as it was saturated with MB particles. As a result, all the adsorption sites of MCC had been used up, and could not further remove the MB dye.

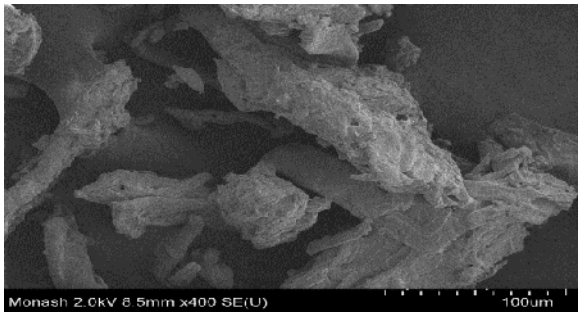


**(a)**

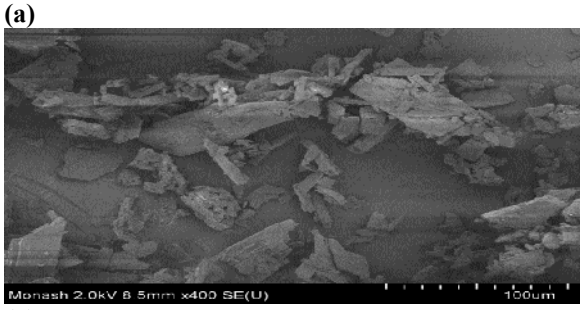


**(b)**

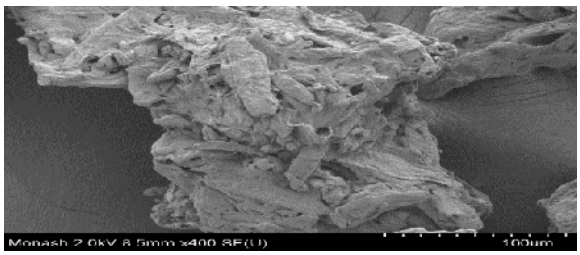


**(c)**

Fig. 12: FE-SEM Images of (a) pure MCC, (b) MB Powder and (c) MCC after 12 minutes of adsorption time (5ppm MB, 5g/L MCC Dosage).

*FTIR*

Fig. 13(a) shows the FTIR spectra of pure MCC before the adsorption process. The wavelength of 3436 $cm^{-1}$ and 1642 $cm^{-1}$ represented the stretching and bending of hydroxyl group respectively in the MCC structure [58]. A peak was observed in 2917$cm^{-1}$ due to the asymmetric stretching vibration of C-H in pyranoid ring, while the stretching of 1057-1033 $cm^{-1}$ represent the C-O-C bond of the cyclic alcohol of cellulose [59]. Fig. 13 (b) demonstrates the FTIR spectra for MB. A sharp peak could be seen at wavelength of 1601 $cm^{-1}$ which represented the C=N-bond in the MB structure while the stretching at 1180-1147 $cm^{-1}$ represented the N-C bond of the aromatic amines functional group in MB structure. There was no hydroxyl functional group exist in MB structure [60]. Therefore, the hydroxyl peak appeared at 3423 $cm^{-1}$ was attributed to the hydrates of the MB powder. The spectrum of MCC after adsorption, which is shown in Fig. 13(c), was very much similar to that of Fig. 13(a). There was still a hydroxyl peak appeared at 3399 $cm^{-1}$ which was due to the moisture of the environment. However higher intensities at 1642 $cm^{-1}$ and 1168-1111 $cm^{-1}$ were observed which are attributed to the overlapping with C=N- bond and N-C bond of the aromatic amines functional group in MB structure, respectively. This showed that MB has been anchored on the surface of the MCC. Comparing Fig. 13(a) and Fig. 13(c), there is neither additional nor disappearance of peaks observed. This verified that there was no chemical adsorption involved. Only electrostatic attraction or physical adsorption involved in the adsorption mechanism.

*Adsorption Mechanism and Future Prospective*

Results have shown that MCC had strong affinity towards MB dye, which led to the rapid

adsorption rate of MB on MCC adsorbent. The strong affinity of MB on MCC was predominantly due to physical adsorption mechanism. As investigated in Section 3.3, the isoelectric point for MCC is at pH 2.8. Thus, the net charge of MCC at pH 2 was positive, due to high concentration of $H^+$ ion. As a result, lowest dye percentage removal was obtained at this pH value due to electrostatic repulsion. Beyond pH 2.8, the net charge of MCC was negative, resulting in significant increase in cationic MB dye percentage removal from pH 2 to pH 3. Thus, the adsorption mechanism of MB on MCC was predominantly due to electrostatic attraction, which was categorized as physical adsorption. This was verified further by Temkin and Dubinin-Radushkevich isotherms and thermodynamics studies, whereby these studies shows that physical adsorption is the predominant adsorption mechanism.

Results from Elovorich kinetics model suggested that there is no chemical adsorption mechanism involved. This was verified by using FTIR on MCC after adsorption, where there was neither additional nor disappearance in peaks. As due to the strong electrostatic interactions between MCC and MB, equilibrium of adsorption occurred at a much faster rate than many other materials. These justified the potential of MCC as sustainable and green adsorbent.

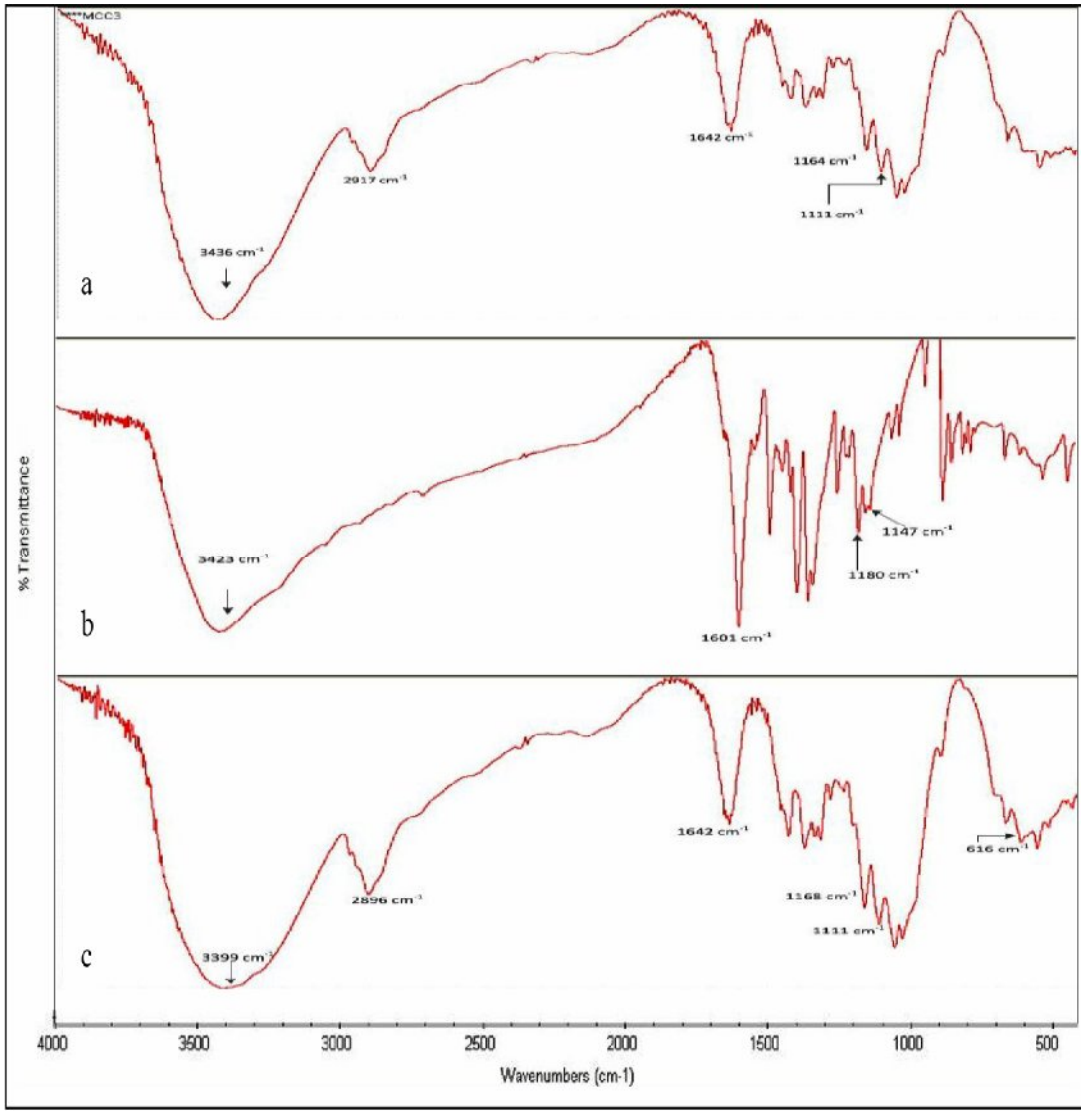


Fig. 13: FTIR of (a) MCC (b) MB (c) MCC after adsorption.

Although this study have been investigated and justify the potential of MCC as sustainable and green adsorbent, there are still some challenges which have to be addressed in the future. The main challenge is the low adsorption capacity. Langmuir isotherm has shown that the maximum adsorption capacity is 4.95 mg/g, which is still significantly lower than other researched adsorbents on MB dye removal. These include carbon nanotube [61], natural palygorskite [62], and bentonite [63] which have 59.7 mg/g, 158.03 mg/g and 168.63 mg/g respectively. The low adsorption capacity was due to the low surface area (1.32 $m^2$/g) of MCC, resulting in inefficient surface contact area between MCC and MB. Adsorption of water soluble dye is only adsorbed on the amorphous region of MCC as it is more hydrophilic than the crystalline region [64]. Therefore, since MCC has high crystallinity of 83%, there were lesser amorphous regions available for the adsorption of dye, which also contributes to the low adsorption capacity of MCC.

Suggested further improvements could be investigated in the future to increase the adsorption capacities. This includes the fabrication of MCC beads [65], which could significantly increase porosity, surface area, decrease crystallinity and improve access to internal sorption sites [66], which in turn, will increase the adsorption capacity of MCC. Similar bio-adsorbents like chitosan has the same problem of low surface area and high crystallinity in powder formed, which were finally solved by fabrication of chitosan bead [67]. Fabrication of cellulose and MCC beads is a well-established method, whereby cellulose is generally dissolved in a mixture of alkaline with urea or thiourea solution, before it is regenerated as cellulose beads in acidic solution [68]. With a high surface area of between 336-470 $m^2$/g, and porosity between 93-95% [65], pure cellulose beads are mostly used for drug encapsulation and delivery [69]. However, there are very limited studies on the application of MB dye adsorption using MCC and cellulose beads, which could be explored in the future.

Highly porous, low density and high surface area of MCC or cellulose-based aerogels [70] could be also fabricated to overcome the challenge on the low adsorption capacity of MCC powder. The formation of aerogel started with the gelation and dissolution of cellulose, followed by solvent exchange with alcohol, and finally drying to form aerogel [71]. The evaporation of alcohol in the drying steps resulting in several voids formation, subsequently highly porous structure consisting of a network of interconnected uniform cellulose is formed [72]. This provides more adsorption sites for the adsorption of MB, and potentially enhances the adsorption capacity significantly. Cellulose-based aerogel is used as a removal of oil by modifying it into hydrophobic aerogel [72], as pure cellulose aerogel is hydrophilic. Its hydrophilicity thus enhances the interaction between pure cellulose and water soluble dye. However, there are also very limited studies on the application of MB dye adsorption using MCC and cellulose-based aerogel, which could be further explored in the future.

## Conclusion

This paper has studied the adsorption mechanisms of MCC, and its potential as green adsorbent. The adsorption equilibrium fitted well with Langmuir Isotherm, which indicated that monolayer adsorption at the homogenous surface of MCC, whereby adsorbed MB molecules do not interact with each other at neighboring adsorption sites. Temkin and Dubinin-Radushkevich isotherms and thermodynamics studies have shown that electrostatic attraction, which was categorized as physical adsorption, was the dominant adsorption mechanism between MCC and MB. It was due to the electrostatic attraction as adsorption mechanism of this adsorption process which resulted more rapid adsorption of MB dye, compared to a lot of materials, This showed the potential of MCC as the future of green and sustainable adsorbent, particularly for the adsorption of dye, although further improvement is still required to enhance the adsorption capacity.

## Acknowledgement

The authors would like to gratefully acknowledge the Ministry of Education Malaysia (MOE) for providing research funding under the FRGS scheme grant number FRGS/2/2013 TK05/MUSM/03/1.

## References

1. Y. Liu, Y. Zheng and A. Wang, Enhanced Adsorption of Methylene Blue from aqueous Solution by chitosan-g-poly (acrylic acid)/Vermiculite Hydrogel Composites, *J. Environ. Sci.*, 22, 486 (2010).
2. C. Z. Liang, S. P. Sun, F. Y. Li, Y. K. Ong, T. S. Chung, Treatment of Highly Concentrated Wastewater Containing Multiple Synthetic Dyes by a Combined Process of Coagulation/Flocculation and Nanofiltration, *J. Membr. Sci.,* **469**, 306 (2014).
3. F. Banat, S. Al-Asheh and M. Qtaishat, Treatment of Waters Colored with Methylene

Blue Dye by Vacuum Membrane Distillation, *Desalination*, 174 (2005).
4. P. Li, G. Zhao, K. Zhao, J. Gao, T. Wu, An Efficient and Energy Saving Approach to Photocatalytic Degradation of Opaque High-Chroma Methylene Blue Wastewater by Electrocatalytic Pre-Oxidation, *Dyes Pigm.*, **92**, 923 (2012).
5. S. Wang, L. Li, H. Wu and Z. H. Zhu, Unburned Carbon as a Low-Cost Adsorbent for Treatment of Methylene Blue-Containing Wastewater, *J. Colloid Interface Sci.*, **292**, 336 (2005).
6. L. Xiong, Y. Yang, J. Mai, W. Sun, C. Zhang, D. Wei, Q. Chen and J. Ni, Adsorption Behavior of Methylene Blue onto Titanate Nanotubes, *Chem. Eng. J.*, **156**, 313 (2010).
7. H. Deng, J. Lu, G. Li, G. Zhang and X. Wang, Adsorption of Methylene Blue on Adsorbent Materials Produced from Cotton Stalk *Chem. Eng. J.*, **172**, 326 (2011).
8. L. Ai, C. Zhang, F. Liao, Y. Wang, M. Li, L. Meng and J. Jiang, Removal of Methylene Blue from Aqueous Solution with Magnetite Loaded Multi-Wall Carbon Nanotube: Kinetic, Isotherm and Mechanism Analysis, *J. Hazard. Mater.,* **198**, 282 (2011).
9. S. K. Theydan, M. J. Ahmed, Adsorption of Methylene Blue onto Biomass-Based Activated Carbon by FeCl3 Activation: Equilibrium, Kinetics, and Thermodynamic Studies, *J. Anal. Appl. Pyrolysis*, **97**, 116 (2012).
10. Y. Li, Q. Du, T. Liu, J. Sun, Y. Wang, S. Wu, Z. Wang, Y. Xia and L. Xia, Methylene Blue Adsorption on Graphene Oxide/Calcium Alginate Composites, *Carbohydr. Polym.,* **95**, 501 (2013).
11. V. Meshko, L. Markovska, M. Mincheva and A. E. Rodrigues, Adsorption of Basic Dyes on Granular Acivated Carbon and Natural Zeolite, *Water Res*., **35**, 3357 (2001).
12. M. Y. Chang and R. S. Juang, Adsorption of Tannic Acid, Humic Acid, and Dyes from Water Using the Composite of Chitosan and Activated Clay, *J. Colloid Interface Sci.,* **278**, 18 (2004).
13. H. Guo, S. Zhang, Z. Kou, S. Zhai, W. Ma, Y. Yang, Removal of Cadmium(II) from Aqueous Solutions by Chemically Modified Maize Straw, *Carbohydr. Polym.,* **115**, 177 (2015).
14. A. Z. Abdullah, B. Salamatinia, A. H. Kamaruddin, Application of Response Surface Methodology for the Optimization of NaOH Treatment on Oil Palm Frond Towards Improvement in the Sorption of Heavy Metals, *Desalination*, **244**, 227 (2009).
15. M. S. Chiou, H. Y. Li, Equilibrium and Kinetic Modeling of Adsorption of Reactive Dye on Cross-Linked Chitosan Beads, *J. Hazard. Mater.,* **93**, 233 (2002).
16. Y. Xing, X. Sun, B. Li, Poly(Methacrylic Acid)-Modified Chitosan for Enhancement Adsorption of Water-Soluble Cationic Dyes, *Polym. Eng. Sci.,* **49**, 272 (2009).
17. M. S. Chiou, H. Y. Li, Equilibrium and Kinetic Modeling of Adsorption of Reactive Dye on Cross-Linked Chitosan Beads, *J. Hazard. Mater.,* **93**, 233 (2002).
18. A. R. Cestari, E. F. S. Vieira, A. G. P. Dos Santos, J. A. Mota, V. P. De Almeida, Adsorption of Anionic Dyes on Chitosan Beads. 1. The Influence of the Chemical Structures of Dyes and Temperature on the Adsorption Kinetics, *J. Colloid Interface Sci.,* **280**, 380 (2000).
19. G. Zhang, L. Yi, H. Deng and P. Sun, Dyes Adsorption using a Synthetic Carboxymethyl Cellulose-Acrylic Acid Adsorbent, *J. Environ. Sci.*, **26**, 1203 (2014).
20. L. Wang, J. Li, Adsorption of C. I. Reactive Red 228 Dye from Aqueous Solution by Modified Cellulose from Flax Shive: Kinetics, Equilibrium, and Thermodynamics, *Ind. Crops Prod.,* **42**, 153 (2013).
21. X. Luo and L. Zhang, High Effective Adsorption of Organic Dyes on Magnetic Cellulose Beads Entrapping Activated Carbon, *J. Hazard. Mater.,* **171**, 340 (2009).
22. L. S. Silva, L. C. B. Lima, F. C. Silva, J. M. E. Matos, M. R. M. C. Santos, L. S. Santos Júnior, K. S. Sousa, E. C. da Silva Filho, Dye Anionic Sorption in Aqueous Solution onto a Cellulose Surface Chemically Modified with Aminoethanethiol, *Chem. Eng. J.*, **218**, 89 (2013).
23. A. L. Cazetta, A. M. M. Vargas, E. M. Nogami, M. H. Kunita, M. R. Guilherme, A. C. Martins, T. L. Silva, J. C. G. Moraes, V. C. Almeida, NaOH-Activated Carbon of High Surface Area Produced from Coconut Shell: Kinetics and Equilibrium Studies from the Methylene Blue Adsorption, *Chem. Eng. J.*, **174**, 117 (2011).
24. J. M. Parnis, K. B. Oldham, Beyond the Beer–Lambert law: The Dependence of Absorbance on Time in Photochemistry, *J. Photochem. Photobiol.,* A., **267**, 6 (2013).
25. Z. Eren, F. N. Acar, Adsorption of Reactive Black 5 from an Aqueous Solution: Equilibrium and Kinetic Studies, *Desalination,* **194**, 1 (2006).
26. M. A. M. Salleh, D. K. Mahmoud, W. A. W. A. Karim, A. Idris, Cationic and Anionic Dye Adsorption by Agricultural Solid Wastes: A Comprehensive Review, *Desalination,* **280**, 1 (2011).

27. M. T. Yagub, T. K. Sen, S. Afroze, H. M. Ang, Dye and its Removal from Aqueous Solution by Adsorption: A review, *Adv. Colloid Interface Sci.,* **209**, 172 (2014).
28. S. Selvakumar, R. Manivasagan, K. Chinnappan, Biodegradation and Decolourization of Textile Dye Wastewater Using Ganoderma Lucidum, 3 *Biotech,* **3**, 71 (2013).
29. B. H. Hameed, A. A. Ahmad, Batch Adsorption of Methylene Blue from Aqueous Solution by Garlic Peel, an Agricultural Waste Biomass, *J. Hazard. Mater.,* **164**, 870 (2009).
30. M. C. Ncibi, B. Mahjoub, M. Seffen, Kinetic and Equilibrium Studies of Methylene Blue Biosorption by *Posidonia oceanica* (L.) Fibres, *J. Hazard. Mater.*, **139**, 280 (2007).
31. F. A. Pavan, A. C. Mazzocato and Y. Gushikem, Removal of Methylene Blue Dye from Aqueous Solutions by Adsorption Using Yellow Passion Fruit Peel as Adsorbent, *Bioresour. Technol.,* **99**, 3162 (2008).
32. C. H. Weng, Y. T. Lin, T. W. Tzeng, Removal of Methylene Blue from Aqueous Solution by Adsorption onto Pineapple Leaf Powder*, J. Hazard. Mater.,* **170**, 417 (2009).
33. A. N. Zhukov, D. Y. Baturenko, Y. M. Chernoberezhskii, A. V. Lorentsson, Conductivity and Electrokinetic Potential of Microcrystalline Cellulose Particles in Aqueous HCl and NaOH Solutions, *Colloid J.,* **65**, 310 (2003).
34. C. H. Giles, T. H. MacEwan, S. N. Nakhwa, D. Smith, 786. Studies in Adsorption. Part XI. A System of Classification of Solution Adsorption Isotherms, and its Use in Diagnosis of Adsorption Mechanisms and in Measurement of Specific Surface Areas of Solids, *J. Chem. Soc.,* 3973 (1960).
35. J. S. Piccin, C. S. Gomes, L. A. Feris, M. Gutterres, Kinetics and Isotherms of Leather Dye Adsorption by Tannery Solid Waste *Chem. Eng. J.*, **183**, 30 (2012).
36. G. Limousin, J. P. Gaudet, L. Charlet, S. Szenknect, V. Barthès, M. Krimissa, Sorption Isotherms: A Review on Physical Bases, Modeling and Measurement, *Applied Geochemistry*, **22**, 249 (2007).
37. I. Langmuir, The Adsorption of Gases on Plane Surfaces of Glass, Mica, and Platinum, *J. Am. Chem. Soc.*, **40**, 1361 (1918).
38. K. R. Hall, L. C. Eagleton, A. Acrivos, T. Vermeulen, Pore- and Solid-Diffusion Kinetics in Fixed-Bed Adsorption under Constant-Pattern Conditions, *Ind. Eng. Chem*, **5**, 212 (1966).
39. S. Wang, Z. H. Zhu, Characterisation and Environmental Application of an Australian Natural Zeolite for Basic Dye Removal from Aqueous Solution, *J. Hazard. Mater.,* **136**, 946 (2006).
40. S. Rangabhashiyam, N. Anu, M. S. Giri Nandagopal, N. Selvaraju, Relevance of Isotherm Models in Biosorption of Pollutants by Agricultural Byproducts, *J. Environ. Chem. Eng.,* **2**, 398 (2014).
41. A. G. El Said, N. A. Badawy, A. Y. Abdel-Aal, S. E. Garamon, Optimization Parameters for Adsorption and Desorption of Zn(II) and Se(IV) using Rice Husk Ash: Kinetics and Equilibrium, Ionics, **17**, 263 (2011).
42. A. Olgun and N. Atar, Equilibrium and Kinetic Adsorption Study of Basic Yellow 28 and Basic Red 46 by a Boron Industry Waste, *J. Hazard. Mater.,* **161**, 148 (2009).
43. A. A. Oladipo, M. Gazi, S. Saber-Samandari, Adsorption of Anthraquinone Dye onto Eco-Friendly Semi-IPN Biocomposite Hydrogel: Equilibrium Isotherms, Kinetic Studies and Optimization, *J. Taiwan Inst. Chem. Eng.*, **45**, 653 (2014).
44. V. V. Panic, S. J. Velickovic, Removal of Model Cationic Dye by Adsorption onto poly(methacrylic acid)/Zeolite Hydrogel Composites: Kinetics, Equilibrium Study and Image Analysis, *Sep. Purif. Technol.,* **122**, 384 (2014).
45. S. S. M. B. Ibrahim, Comparative Isotherms Studies on Adsorptive Removal of Congo Red from Wastewater by Watermelon Rinds and Neem-Tree Leaves, *Open J Phys Chem.*, **4**, 139 (2014).
46. H. El Boujaady, M. Mourabet, M. Bennani-Ziatni, A. Taitai, Adsorption/Desorption of Direct Yellow 28 on Apatitic Phosphate: Mechanism, Kinetic and Thermodynamic Studies, *J. Asso. Arab. Uni. Basic. App. Sci.,* **16**, 64 (2014).
47. N. M. Mahmoodi, B. Hayati, M. Arami and C. Lan, Adsorption of Textile Dyes on Pine Cone from Colored Wastewater: Kinetic, Equilibrium and Thermodynamic Studies, *Desalination,* **268,** 117 (2011).
48. H. Chen, J. Zhao, J. Wu and G. Dai, Isotherm, Thermodynamic, Kinetics and Adsorption Mechanism Studies of Methyl Orange by Surfactant Modified Silkworm Exuviae, *J. Hazard. Mater.*, **192**, 246 (2011).
49. S. Wang, C. W. Ng, W. Wang, Q. Li and L. Li, A Comparative Study on the Adsorption of Acid and Reactive Dyes on Multiwall Carbon Nanotubes in Single and Binary Dye Systems, *J. Chem. Eng. Data*, **57**, 1563 (2012).

50. Y. H. Chen, Synthesis, Characterization and Dye Adsorption of Ilmenite Nanoparticles, *J. Non-Cryst. Solids*, **357**, 136 (2011).
51. K. Bubacz, B. Tryba, A. W. Morawski, The Role of Adsorption in Decomposition of Dyes on $TiO_2$ and N-modified TiO2 Photocatalysts Under UV and Visible Light Irradiations, *Mater. Res. Bull.*, **47**, 3697 (2012).
52. A. Z. Aroguz, J. Gulen, R. H. Evers, Adsorption of Methylene Blue from Aqueous Solution on Pyrolyzed Petrified Sediment, *Bioresour. Technol.,* **99**, 1503 (2008).
53. P. R. Rout, P. Bhunia, R. R. Dash, Modeling Isotherms, Kinetics and Understanding the Mechanism of Phosphate Adsorption onto a Solid Waste: Ground Burnt Patties, *J. Environ. Chem. Eng.*, **2**, 1331 (2014).
54. A. H. Chen, Y. Y. Huang, Adsorption of Remazol Black 5 from Aqueous Solution by the Templated Crosslinked-Chitosans, *J. Hazard. Mater.,* **177**, 668 (2010).
55. F. C. Wu, R. L. Tseng and R. S. Juang, Characteristics of Elovich Equation Used for the Analysis of Adsorption Kinetics in Dye-Chitosan Systems, *Chem. Eng. J.*, **150**, 366 (2009).
56. K. Pyrzyńska, M. Bystrzejewski, Comparative Study of Heavy Metal Ions Sorption onto Activated Carbon, Carbon Nanotubes, and Carbon-Encapsulated Magnetic Nanoparticles, *Colloids Surf.,* A*,* **362**, 102 (2010).
57. S. Brunauer, P. H. Emmett, E. Teller, Adsorption of Gases in Multimolecular Layers, *J. Am. Chem. Soc.*, **60**, 309 (1938).
58. Z. Shan, W. S. Yang, X. Zhang, Q. M. Huang and H. Ye, Preparation and Characterization of Carboxyl-Group Functionalized Superparamagnetic Nanoparticles and the Potential for Bio-Applications, *J. Braz. Chem. Soc.*, **18**, 1329 (2007).
59. M. Kačuráková, P. Capek, V. Sasinková, N. Wellner, A. Ebringerová, FT-IR Study of Plant Cell Wall Model Compounds: Pectic Polysaccharides and Hemicelluloses, *Carbohydr. Polym.,* **43**, 195 (2000).
60. P. Zugenmaier, Crystalline Cellulose and Derivatives, in: R. W. T. E. Timell (Ed.), Springer, Clausthal-Zellerfeld, Germany, 2008, pp. 286.
61. Y. Yao, F. Xu, M. Chen, Z. Xu and Z. Zhu, Adsorption Behavior of Methylene Blue on Carbon Nanotubes, *Bioresour. Technol.*, **101**, 3040 (2010).
62. Y. Zhang, W. Wang, J. Zhang, P. Liu and A. Wang, A Comparative Study About Adsorption of Natural Palygorskite for Methylene Blue, *Chem. Eng. J.*, **262**, 390 (2015).
63. Y. Liu, Y. Kang, B. Mu, A. Wang, Attapulgite/Bentonite Interactions for Methylene Blue Adsorption Characteristics from Aqueous Solution, *Chem. Eng. J.*, **237**, 403 (2014).
64. G. Thoorens, F. Krier, B. Leclercq, B. Carlin and B. Evrard, Microcrystalline Cellulose, a Direct Compression Binder in a Quality by Design Environment—A review, *Int. J. Pharm.,* **473**, 64 (2014).
65. J. Trygg, P. Fardim, M. Gericke, E. Mäkilä and J. Salonen, Physicochemical Design of the Morphology and Ultrastructure of Cellulose Beads, *Carbohydr. Polym.*, **93**, 291 (2013).
66. P. Miretzky, A. F. Cirelli, Hg(II) Removal from Water by Chitosan and Chitosan Derivatives: A review, *J. Hazard. Mater.,* **167**, 10 (2009).
67. M. Vakili, M. Rafatullah, B. Salamatinia, A. Z. Abdullah, M. H. Ibrahim, K. B. Tan, Z. Gholami, P. Amouzgar, Application of Chitosan and its Derivatives as Adsorbents for Dye Removal from Water and Wastewater: A Review, *Carbohydr. Polym.,* **113**, 115 (2014).
68. B. Medronho, B. Lindman, Brief Overview on Cellulose Dissolution/Regeneration Interactions and Mechanisms, *Adv. Colloid Interface Sci.,* (2014).
69. J. Trygg, E. Yildir, R. Kolakovic, N. Sandler, P. Fardim, Anionic Cellulose Beads for Drug Encapsulation and Release, *Cellulose,* **21**, 1945 (2014).
70. T. Oshima, T. Sakamoto, K. Ohe and Y. Baba, Cellulose Aerogel Regenerated from Ionic Liquid Solution for Immobilized Metal Affinity Adsorption, *Carbohydr. Polym*, **103**, 62 (2014).
71. H. Jin, Y. Nishiyama, M. Wada, S. Kuga, Nanofibrillar Cellulose Aerogels, *Colloids Surf.,* A*,* **240**, 63 (2004).
72. S. T. Nguyen, J. Feng, N. T. Le, A. T. T. Le, N. Hoang, V. B. C. Tan, H. M. Duong, Cellulose Aerogel from Paper Waste for Crude Oil Spill Cleaning, *Ind. Eng. Chem. Research*, **52**, 18386 (2013).